Hindawi Publishing Corporation
Journal of Spectroscopy
Volume 2015, Article ID 356027, 16 pages
http://dx.doi.org/10.1155/2015/356027

Research Article

Influence of the Chemical Composition in the Electrochemical Response of Permanent Magnets

S. Godavarthi,[1] J. Porcayo-Calderon,[2] E. Vazquez-Velez,[1] M. Casales-Diaz,[1] D. M. Ortega-Toledo,[1,3] and L. Martinez-Gomez[1,3]

[1] *Instituto de Ciencias Físicas, Universidad Nacional Autónoma de México, Avenida Universidad s/n, 62210 Cuernavaca, MOR, Mexico*
[2] *CIICAp, Universidad Autónoma del Estado de Morelos, Avenida Universidad 1001, 62209 Cuernavaca, MOR, Mexico*
[3] *Corrosion y Protección (CyP), Buffon 46, 11590 Mexico City, DF, Mexico*

Correspondence should be addressed to J. Porcayo-Calderon; jporcayoc@gmail.com

Received 17 August 2015; Revised 25 October 2015; Accepted 1 November 2015

Academic Editor: Michele Fedel

The corrosion behavior of permanent magnets with different chemical composition was evaluated. Permanent magnets were tested in 3.5% NaCl solution at room temperature using electrochemical technics such as polarization curves, open-circuit potential, linear polarization resistance, and electrochemical impedance spectroscopy measurements. Results have shown that corrosion rate is affected by Nd, Pr, and Co content. Analysis by scanning electron microscopy has shown that pitting attack is the main mode of degradation of the magnets, while Co addition reduces it and Pr addition increases it.

1. Introduction

Rare earth elements are increasingly playing significant role in development of new functional materials. For example, Nd is key element for making important types of permanent magnets. These permanent magnets are necessary components in a lot of the electric, electronic, and electromechanical devices used in today's technology. The purpose of these materials is to provide large magnetic fields without the expenditure of electrical power or the generation of heat. Based on type of the materials used for manufacturing the permanent magnets, they can be classified as alnico, ferrite, rare earth-cobalt, and rare earth-iron. NdFeB magnets have the highest energy product $(BH)_{max}$ of all permanent magnet material ever developed, but they are sensitive to the temperature and corrosiveness of the working environment [1]. NdFeB permanent magnets can be manufactured by powder metallurgical processing or by bonding magnetic particles in a polymer matrix [2].

NdFeB sintered magnets have been widely applied in various industries because of their remarkable magnetic properties [2]. However, these types of magnets could not be used for some commercial applications due to their very low resistance against corrosion in various ambient environments [3–5]. This very low resistance against corrosion of NdFeB sintered magnets may be attributed to the existence of complex multiple phases in their microstructure. The most important ferromagnetic phase present in NdFeB sintered magnets is the compound $Nd_2Fe_{14}B$ (matrix phase, ϕ-phase). The ferromagnetic phase (tetragonal compound $Nd_2Fe_{14}B$) is surrounded by low corrosion resistant intergranular regions containing Nd_4Fe (neodymium-rich phase, n-phase) and $Nd_{(1+\varepsilon)}Fe_4B_4$ (boron-rich phase, η-phase) [6]. Fidler [7] indicated that it is possible for a single magnet to have different types of the Nd-rich phase, where the main Fe : Nd stoichiometric ratios may be 1 : 1.2–1.4, 1 : 2.0–2.3, 1 : 3.5–4.4, and >1 : 7. The Nd-rich and B-rich phases are located in the intergranular regions surrounding the matrix grains, and their volume fractions are around 10% and 7%, respectively.

However, the Nd-rich phase has a poor corrosion resistance; its electrochemical activity is highest. The anodic dissolution of the Nd-rich phase occurs at more active potentials than the corrosion potential of the NdFeB magnet [8]. The dissolution of the Nd-rich phase can provoke the disintegration of the magnet [9]. Corrosion performance of permanent magnets is carried out by immersion in a neutral

salt solution or a neutral salt spray test. It has been shown that, in a neutral NaCl solution, the corrosion rates of the uncoupled single phases are different, for the reason that the Nd-rich phase has the lowest corrosion resistance and the matrix phase the highest one [5]. The electrochemical potentials of the present phases lead to galvanic corrosion, resulting in preferential corrosion by grain boundary. This is because the area fraction of the anode (Nd-rich phase and B-rich phase) is much smaller than that of the matrix phase (cathode), thereby accelerating corrosion of the anode [10, 11].

It is said that Nd can absorb H_2 evolved by the corrosion process, and this can lead to an expansion of the Nd-rich phase causing the embrittlement of the permanent magnet and finally its pulverization [9, 12, 13]. Extensive research has been carried out to improve the performance of the permanent magnets, for example, increasing the Curie temperature by modification of the chemical composition (substituting Fe by other elements) and increasing the corrosion resistance by either applying protective coatings or adding alloying elements to the substrate [14]. However, this is always accompanied by a sacrifice of the magnetic properties, and the protective coatings are not perfect barriers. For this reason the NdFeB magnets have a poor corrosion resistance in moist environments. In general, the Nd-rich phase catalyzes the formation of H_2 from H_2O and then H_2 forms a hydride with the Nd-rich phase causing its disintegration. Therefore, if an uncoated NdFeB magnet is used, it will be corroded within weeks. This is the reason why the magnets are coated with Ni or Ni-Cu-Ni layer [15].

The aim of the present work is intended to study the corrosion resistance of commercial permanent magnets with different chemical composition in 3.5% NaCl solution at room temperature by applying electrochemical techniques.

2. Experimental Procedure

50 NdFeB magnets obtained from computer hard disks of various brands were analyzed and then classified according to elemental chemical composition. The compositions selected for testing are shown in Table 1. In general the chemical composition of NdFeB magnets varies depending on its final application. For example, permanent magnets for high temperature environments contain Dy or Ho, or Pr can partially replace Nd. Because Nd and Pr differ by only one atomic number, during the extraction process Nd and Pr are not separated completely [15].

For simplicity hereinafter, the first group of magnets (35Nd, 40Nd, and 40Nd3Co) will be defined as Nd magnets and the second one (30Nd6Pr, 30Nd8Pr, and 30Nd10Pr) as NdPr magnets.

In order to demagnetize the magnets, they were thermally treated at 200°C for 2 hours in a muffle furnace and then the specimens were welded to a copper wire as an electrical contact using the spot-welding technique to one of their surfaces. The magnets were then cold mounted in epoxy resin. Wet grinding technique was employed to grind the samples with 120-grit to 600-grit SiC paper. All the samples before exposure to the test corrosion were degreased with ethanol in an ultrasonic bath, dried in air, and stored prior to testing.

Table 1: Chemical compositions of the magnets tested in 3.5% NaCl solution at 25°C.

Magnet	Chemical composition (wt.%)			
	Nd	Pr	Co	(Fe + B)
35Nd	34.76	—	—	Balance
40Nd	39.79	—	—	Balance
40Nd3Co	39.41	—	3.18	Balance
30Nd6Pr	30.46	5.95	—	Balance
30Nd8Pr	29.70	8.15	—	Balance
30Nd10Pr	29.96	9.96	—	Balance

Electrochemical measurements were carried out in a Gamry Interface 1000 Potentiostat controlled by a personal computer. All the experiments were performed in a standard three-electrode cell arrangement with the magnets as working electrode, together with a saturated calomel electrode (SCE) as the reference electrode and a high-purity graphite rod as the auxiliary electrode. Electrochemical measurements were made using at least 100 mL of electrolyte in accordance with ASTM G31-90. Corrosion performance was determined in 3.5 wt.% NaCl aqueous solution at 25°C for 24 hours.

Open-circuit potential (E_{corr}), current density (I_{corr}), and Tafel slopes (b_a, b_c) were determined by means of potentiodynamic polarization curves. The potential scanning range was from −400 mV to 400 mV from the E_{corr} value in accordance with ASTM G5-04 and ASTM G-3-04. A sweep rate of 1 mV/s was used for all the tests to obtain steady-state current-potential curves [16]. Before starting the test the system was kept stabilizing for a period of 0.5 hours.

The linear polarization resistance (LPR) measurements were carried out by polarizing the working electrode from −20 mV to 20 mV from the E_{corr} value with a sweep rate of 60 mV/min and the intensity ΔI was registered in accordance with ASTM G59-97 standard recommended practice. The measurements were recorded every one hour for 24 hours. The value of the polarization resistance (R_p) was deduced from the equation $R_p = \Delta E/\Delta I$, where ΔE is the step of the potential applied at the corrosion potential and ΔI is the resulting current. After determining the polarization resistance, the corrosion current densities (I_{corr}) can be calculated by applying the Stern-Geary equation ($I_{corr} = B/R_p$), where the values of b_a and b_c were previously obtained (see (1) and (2)):

$$\left[\frac{d(\Delta E)}{di}\right]_{\Delta E=0} = R_p = \frac{b_a b_c}{2.303\left(b_a + b_c\right) I_{corr}}, \quad (1)$$

$$I_{corr} = \frac{b_a b_c}{2.303 R_p \left(b_a + b_c\right)}. \quad (2)$$

Electrochemical impedance spectroscopy (EIS) measurements were made at frequencies from 0.01 Hz to 100,000 Hz with a small amplitude sinusoidal potential perturbation signal of ±10 mV. After the corrosion tests, the surface

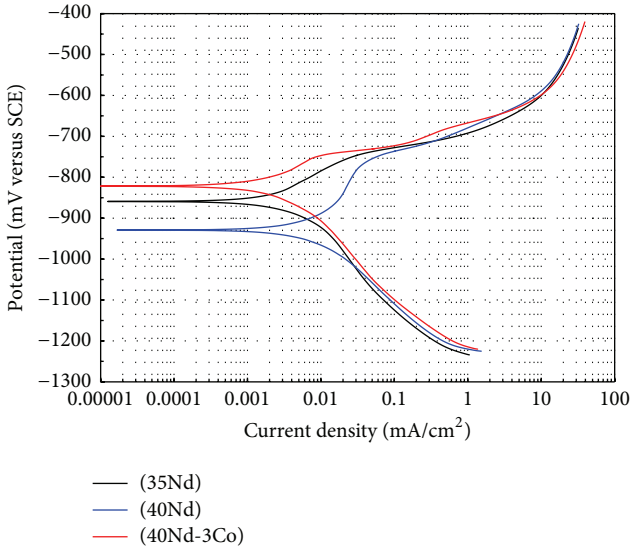

Figure 1: Potentiodynamic polarization curves of the Nd magnets tested in 3.5% NaCl solution at 25°C.

morphology of the corroded sintered magnets was analyzed with a Hitachi SU1510 scanning electron microscopy (SEM).

3. Results and Discussion

3.1. Potentiodynamic Polarization Curves. Figure 1 shows characteristic potentiodynamic current density-potential curves (polarization curves) of the Nd magnets when immersed in 3.5 wt.% NaCl solutions at 25°C for 24 hours. In the anodic region, the 35Nd magnet shows an active dissolution process in the entire potential range. It is observed that increasing the Nd content (40Nd magnet) displaced the polarization curve to more active potential with an increase in I_{corr} value and favoring the apparent formation of a passive zone. Furthermore, the addition of Co (40Nd3Co magnet) causes a shift of the polarization curve to nobler potentials, with a decrease in I_{corr} value and the apparent disappearance of passive region.

The different phases present in the permanent magnets are Nd-rich phase (grain boundary), $Nd_{1+\varepsilon}Fe_4B_4$ (B-rich phase), and $Nd_2Fe_{14}B$ (matrix phase). Because the electrical potential of the Nd-rich phase is much more negative than that of the other phases, the Nd-rich phase oxidizes to Nd^{3+}. Nd^{3+} can be combined with OH^- or with water to form an insoluble precipitate of $Nd(OH)_3$. At the same time, H^+ produced by H_2O dissociation is reduced onto both the B-rich phase and the matrix phase. Part of the hydrogen ions is evolved as H_2, causing the breaking of the corrosion products layer. On the other hand, the atomic hydrogen can be absorbed by the matrix phase, resulting in the lattice expansion and therefore decreasing its magnetic properties [17, 18]. It is known that, in aqueous NaCl solution, the dissolution reaction of the Nd-rich phase takes place according to the following anodic reaction [19, 20]:

$$Nd \longrightarrow Nd^{3+} + 3e^- \quad (3)$$

$$Nd^{3+} + 3OH^- \longrightarrow Nd(OH)_3 \quad (4)$$

Table 2: Electrochemical parameters of the Nd magnets tested in 3.5% NaCl solution at 25°C for 24 hours.

Magnet	E_{corr} (mV)	b_a (mV/Dec)	b_c (mV/Dec)	I_{corr} (mA/cm^2)
35Nd	−858	72	227	0.0058
40Nd	−929	246	164	0.0083
40Nd3Co	−820	62	194	0.0033

Table 3: Electrochemical parameters of the NdPr magnets tested in 3.5% NaCl solution at 25°C for 24 hours.

Magnet	E_{corr} (mV)	b_a (mV/Dec)	b_c (mV/Dec)	I_{corr} (mA/cm^2)
30Nd-6Pr	−877	187	152	0.0039
30Nd-8Pr	−902	253	160	0.0044
30Nd-10Pr	−955	315	131	0.0054

$Nd(OH)_3$ formation will decrease the corrosion rate, but Cl^- ions will break the passivation film, accelerating the dissolution process. On the other hand, the cathodic reaction includes two processes, the H_2-evolution reaction and the O_2-consuming reaction. Where the H_2-evolution reaction occurs first, the H^+ concentration decreases, and at the same time the O_2 concentration increases until the initiation of the O_2-consuming reaction:

$$2H^+ + 2e^- \longrightarrow H_2 \uparrow \quad (5)$$

$$O_2 + 2H_2O + 4e^- \longrightarrow 4OH^- \quad (6)$$

OH^- ions will react with Nd^{3+} ions and probably Fe ions causing the deposition of an insoluble corrosion product, mainly $Nd(OH)_3$ [18]. The decomposition of the neodymium hydroxide can occur in two stages as follows [19]:

$$Nd(OH)_3 \longrightarrow NdO(OH) + H_2O \quad (7)$$

$$2NdO(OH) \longrightarrow Nd_2O_3 + H_2O \quad (8)$$

Figure 2 shows the polarization curves for the NdPr magnets measured in 3.5 wt.% NaCl solution at 25°C for 24 hours. The magnets tested in this case have the same Nd content but differ in Pr content. In this case, a behavior very similar in the three curves is observed; however it can be observed that increasing Pr content shifted the curves to more active region, along with increased I_{corr} values. By comparing the behavior of the 35Nd magnet (Figure 1) with that shown by the 30Nd6Pr magnet, it is observed that the 30Nd6Pr magnet shows a smaller increase in the current density by increasing the applied potential (above E_{corr} value). This behavior is more pronounced with increasing the Pr content, and an apparent passivation area can be observed.

Tables 2 and 3 show electrochemical parameters obtained from the potentiodynamic polarization curves of Nd magnets and NdPr magnets exposed to 3.5 wt.% NaCl solutions at 25°C for 24 hours, respectively. A shift of the entire polarization curve towards the region of low current density together with highest potential indicates better corrosion behavior of magnets.

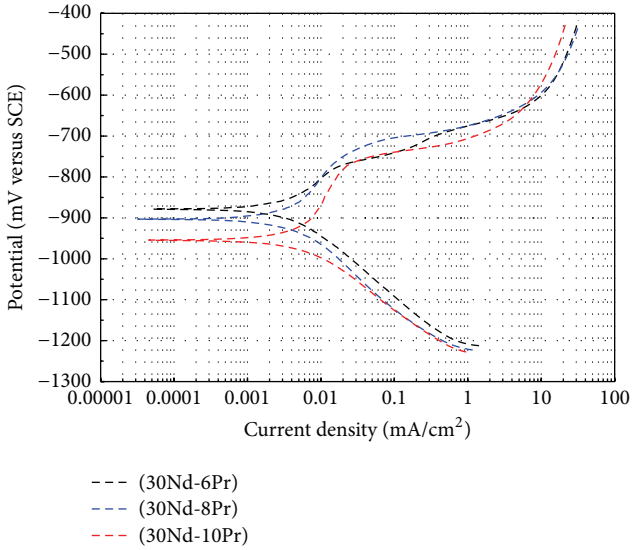

FIGURE 2: Potentiodynamic polarization curves for NdPr magnets exposed to 3.5% NaCl solutions at 25°C for 24 hours.

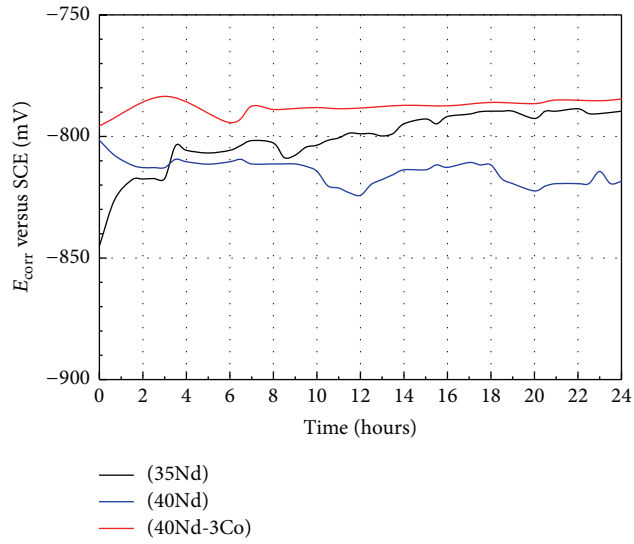

FIGURE 3: Variation of E_{corr} for Nd magnets tested in 3.5% NaCl solution at 25°C for 24 hours.

According to Faraday's law, the relationship between the corrosion rate and the corrosion current density is

$$\upsilon = \frac{MI_{corr}}{nF}, \tag{9}$$

where υ is the corrosion rate, M is the atomic weight of corroding metal, n is the chemical valence state, and F is the Faraday constant. Equation (9) indicates that the corrosion rate is directly proportional to the corrosion current density. Therefore, using the results of potentiodynamic polarization curves, it is possible to consider the following: (i) increasing the Nd content decreases the corrosion resistance of the magnets; (ii) for the same Nd content, the addition of Co improves the corrosion resistance of the magnet; (iii) for the same content of Nd, the addition of Pr improves the corrosion resistance of the magnet; (iv) for the same content of Nd, however, increasing the Pr content increases the corrosion rate of the magnet.

The low corrosion resistance of the magnets can be attributed to the high content of neodymium and to their complex multiphase microstructure. The microstructure comprises ferromagnetic phase matrix ($Nd_2Fe_{14}B$) and the most corrosion sensitive Nd- and B-rich phases in the grain boundary region as explained before. Generally, the corrosion performance observed in the polarization curves is only valid by the beginning of the corrosion process; the observed trend may vary in long time immersion tests [21–23].

3.2. Open-Circuit Potential Measurements. The knowledge of the chemical stability between a metallic material and the electrolyte is essential, and this can be done by monitoring the open-circuit electrode potential (E_{corr}) as a function of time.

An increase in E_{corr} values indicates the formation of a passive film and, otherwise, indicates its breakdown or dissolution, and E_{corr} steady indicates that the film is protective [21–25].

The open-circuit potential (E_{corr}) as a function of time for the Nd magnets tested in 3.5% NaCl solution at 25°C for 24 hours is shown in Figure 3. The 35Nd magnet showed a steady increase in its E_{corr} values without reaching stabilization throughout the test period; this indicates a constant attempt of forming a passive layer onto the surface of the magnet. Any increase in the content of Nd (40Nd magnet) changes the behavior of the magnet to more active potential with a slight tendency to decrease its E_{corr} values over the entire test period. However, for the same content of Nd and with the addition of Co (40Nd3Co magnet) a shift to a nobler potential is observed, and after 8 hours of immersion a stable performance is obtained. These trends are consistent with the observations noted in potentiodynamic polarization curves. Figure 4 shows the effect of Pr content in NdPr magnets on E_{corr}, when tested in 3.5% NaCl solution at 25°C for 24 hours. Trends of E_{corr} values are similar for the three magnets tested, showing a steady decline until 16 hours and then a slight increase. With a higher content of Pr, E_{corr} values are shifted to more active values. Besides, the variation in E_{corr} values is also lower by increasing the content of Pr. These trends are coherent with the potentiodynamic polarization results.

3.3. Linear Polarization Resistance Measurements. Figure 5 shows the variation of the corrosion current density (I_{corr}) for the Nd magnets tested in 3.5% NaCl solution at 25°C for 24 hours. I_{corr} values were obtained from the Stern-Geary equation (see (1)) using Tafel slopes and R_p data (Tables 2 and 3). Variation in I_{corr} values indicates that increasing the content of Nd increases its corrosion rate and the fluctuations in I_{corr} values may be associated with pitting. Furthermore, Co addition significantly increases the

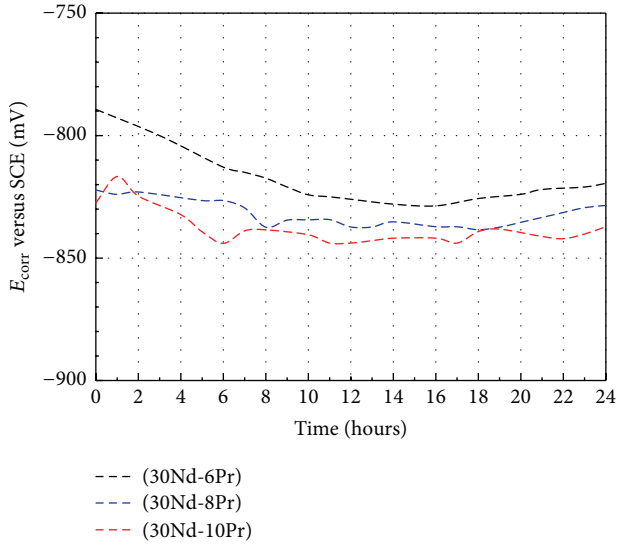

FIGURE 4: Variation of E_{corr} for NdPr magnets tested in 3.5% NaCl solution at 25°C for 24 hours.

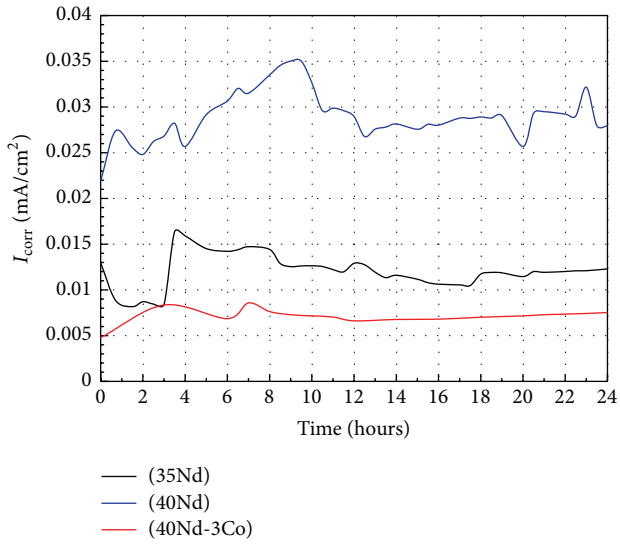

FIGURE 5: Variation of I_{corr} values for Nd magnets tested in 3.5% NaCl solution at 25°C for 24 hours.

corrosion resistance of the magnets, and variations in I_{corr} values are insignificant, possibly indicating a decrease in the pitting attack. These observations are consistent with the results of potentiodynamic polarization curves and open-circuit potential measurements. Figure 6 shows the variation in corrosion current density (I_{corr}) values for NdPr magnets evaluated in 3.5% NaCl solution at 25°C for 24 hours. By comparing the behavior of the 35Nd magnet (Figure 5) with that shown by the 30Nd6Pr magnet, it is observed that both magnets show similar corrosion rates; that is, the Pr addition increased the corrosion rate of the magnets. This behavior is evident noting that for a fixed Nd content the variation in I_{corr} values indicates that increasing the Pr content increases

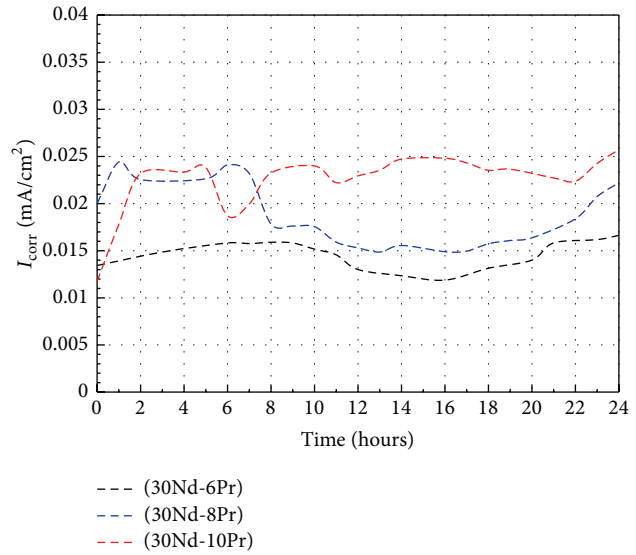

FIGURE 6: Variation of I_{corr} values for NdPr magnets tested in 3.5% NaCl solution at 25°C for 24 hours.

the corrosion rate. This behavior is consistent with the trends observed in E_{corr} values and polarization curves.

3.4. Electrochemical Impedance Spectroscopy Measurements. Electrochemical impedance spectroscopy (EIS) is a very interesting tool because of its advantages: (1) the studying system experiences only a minor disturbance from equilibrium and (2) the evolution and interpretation of the impedance spectra can provide access to the phenomena occurring onto the metallic surface. After converting the data into the frequency domain, it is possible to adapt to an equivalent circuit where the components represent specific parts of the studied system. This technique is sufficient for understanding material behavior since it allows studying both the current and the transfer impedance. Therefore, the impedance measurements technique is one of the more useful methods in order to study the corrosion processes [26, 27]. The specimen response to a small amplitude signal depends on the signal frequency. The variation of impedance modulus and phase angle at each frequency is recorded and the corrosion response of the specimen is expressed as a combination of resistive, capacitive, and inductive components. In general, Bode plots can be interpreted according to the three regions referred to as regions of high, intermediate, and low frequency [28]. (1) High frequency region (1,000–100,000 Hz): in this region, the Bode plot exhibits a constant high frequency plateau (horizontal line) of the $|Z|$ values at $f > 10^4$ Hz, with the phase angle approaching 0°. This is the characteristic response of the resistive region, which includes the electrolyte resistance, R_s, cell geometry, impedance of the conductors, and the reference electrode. (2) Intermediate frequency region (1,000–10 Hz): in the intermediate frequency region, the spectra display a linear slope about −1 in $\log|Z|$ as $\log(f)$ decreases, while the maximum phase angle values approach −90°. This is the characteristic impedance response of the capacitive behavior (Cp) of a compact passive oxide and

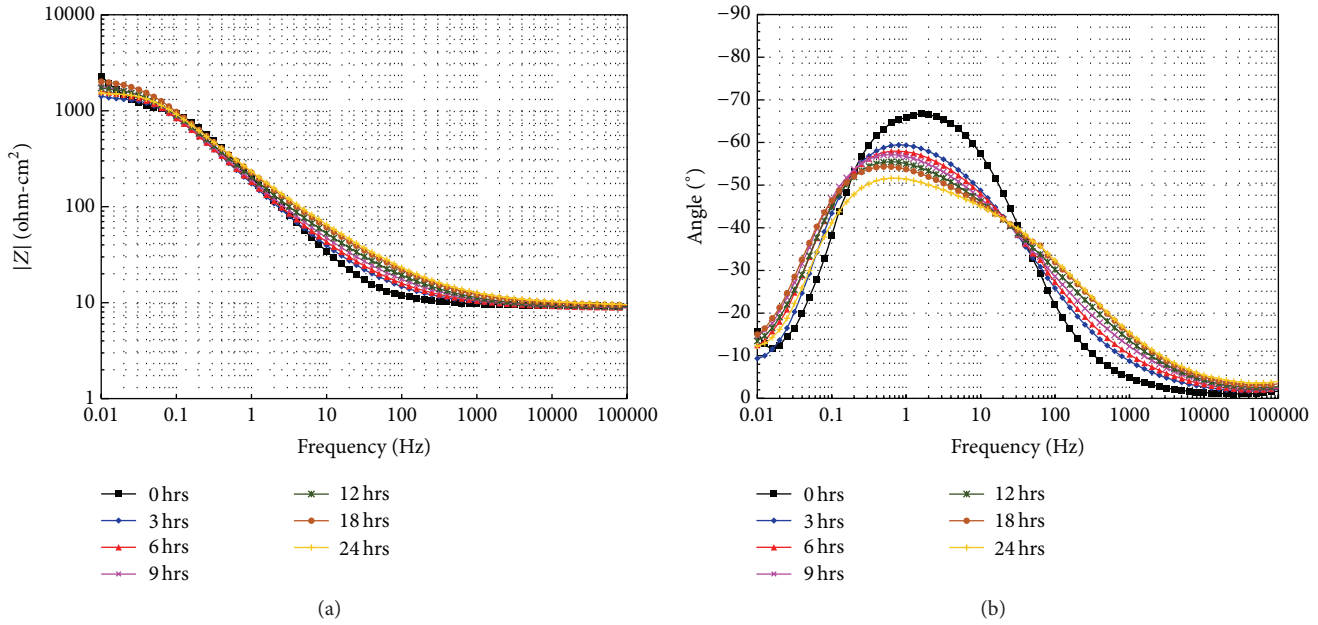

Figure 7: Bode plots for 35Nd magnet tested in 3.5% NaCl solution at 25°C for 24 hours.

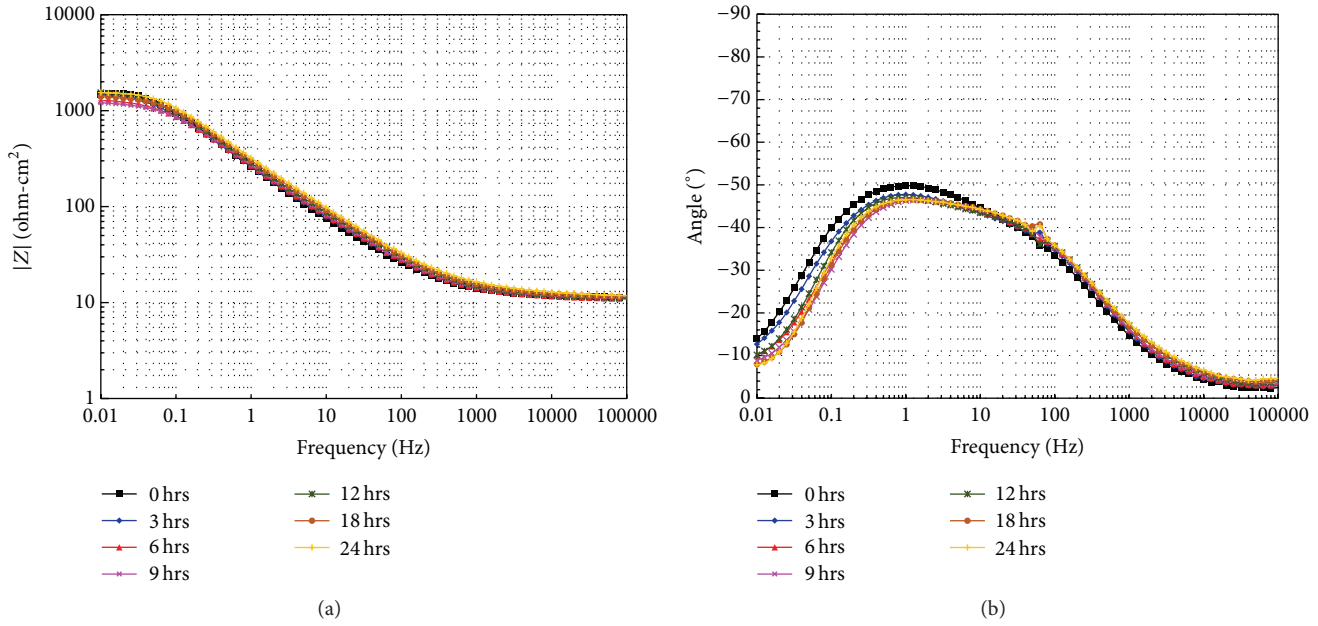

Figure 8: Bode plots for 40Nd magnet tested in 3.5% NaCl solution at 25°C for 24 hours.

describes its dielectric properties. (3) Low frequency region ($f < 10$ Hz): in this region processes are detected such as charge transfer, mass transfer (diffusion or migration), or relaxation taking place at the film-electrolyte interface or within the pores of the surface film.

Results in Bode format of EIS tests, for the Nd magnets in 3.5% NaCl solution at 25°C for 24 h, are presented in Figures 7–10. For 35Nd magnet (Figure 7), in the high frequency region ($f \geq 1000$ Hz) the log $|Z|$ values tend to a constant and the phase angle decreases to zero. The constant value (plateau region) corresponds to the solution resistance (R_s). In the intermediate frequency (around 100 Hz) a new time constant is formed as time evolved. This may be due to the reaction products which accumulate onto the surface of the magnet, according to reactions (3) and (4) previously described [18, 19]. However, this hydroxides' layer did not form a passive film capable of reducing the corrosion rate. Possibly due to that, the aggressive Cl^- ions were absorbed and migrated toward the interface and therefore destroyed the passive film, increasing the dissolution of the magnet. On the other

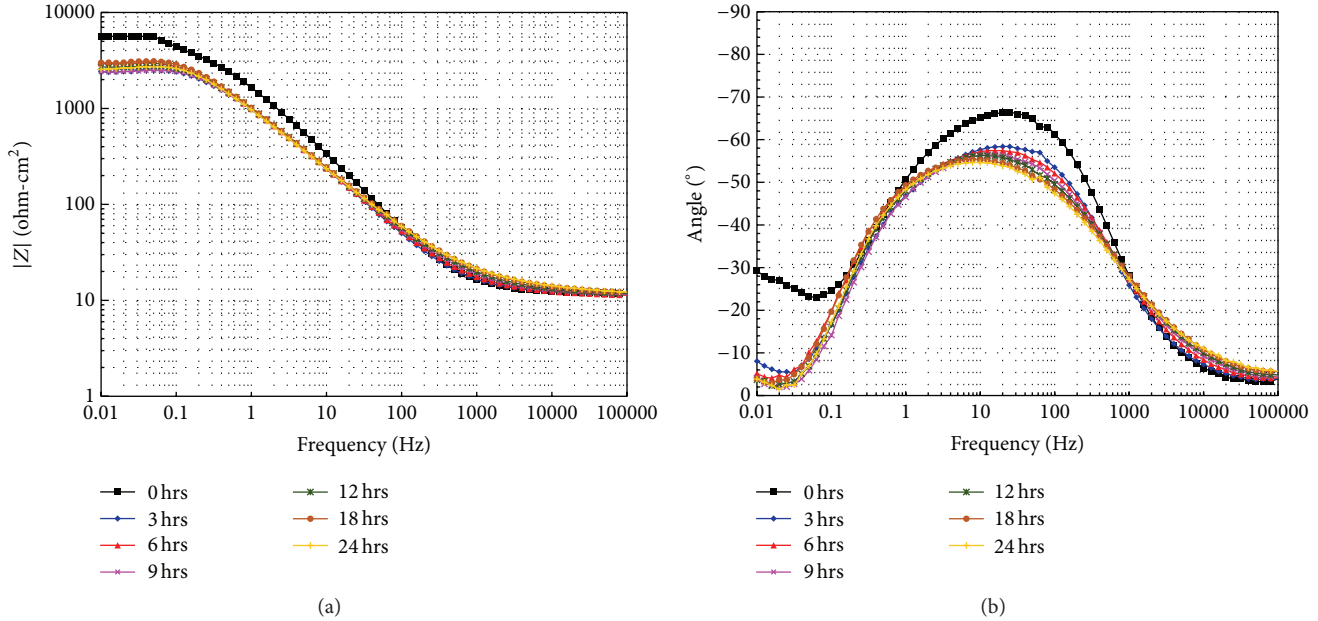

Figure 9: Bode plots for 40Nd3Co magnet tested in 3.5% NaCl solution at 25°C for 24 hours.

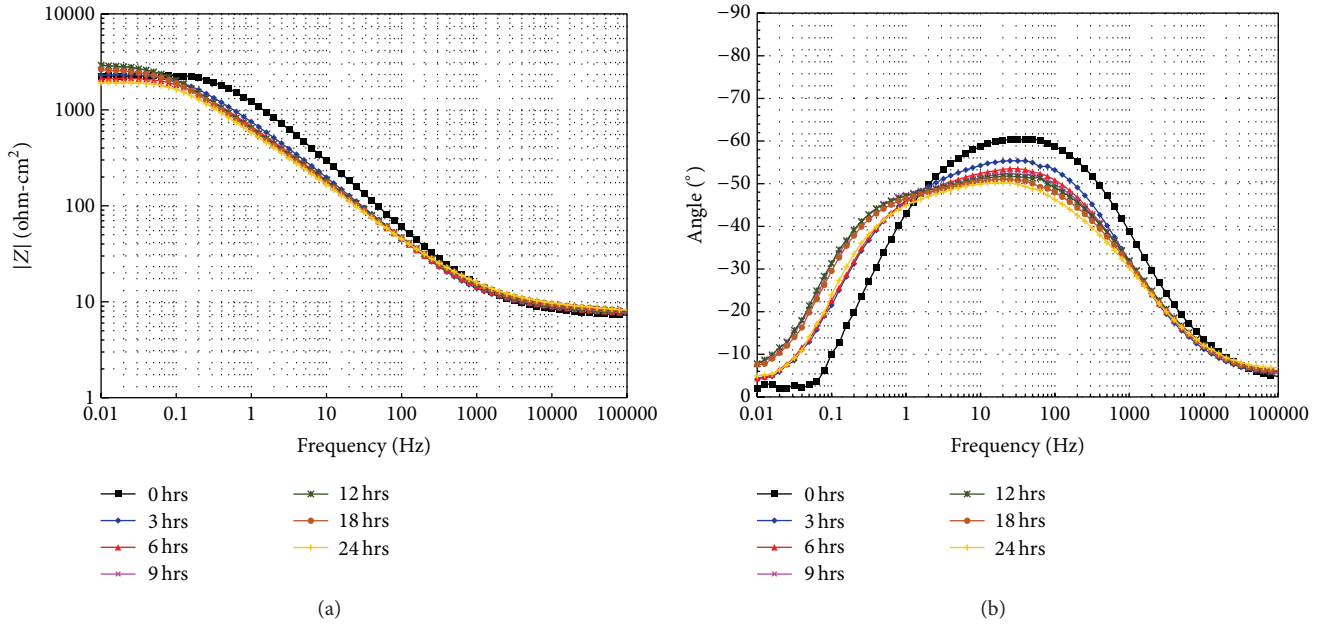

Figure 10: Bode plots for 30Nd6Pr magnet tested in 3.5% NaCl solution at 25°C for 24 hours.

hand, between the intermediate and lower frequency region, a linear relationship between $\log|Z|$ and $\log f$ is observed. The slope value of this linear relationship is lower than −1 and the phase angle value less than 90°, indicating that the protective layer formed has no capacitive nature and that the corrosion process can be under mixed control (diffusion and charge transfer). The maximum phase angle value is shifting toward lower frequencies, and its value also decreases as time passes. These changes can be associated with a detachment, or thinning of the protective films [29, 30], and agree with that described above, because the chloride ions increase the dissolution of the magnet. In the low frequency region, a plateau zone is formed and as time elapses, the $\log|Z|$ values show a tendency to decrease. This indicates the nonprotective nature of the protective layers formed onto magnet surface. Some authors suggest that the increase in the corrosion rate is due to an active dissolution process as a result of the adsorption of the chloride ions which promote the pitting attack until the magnet is completely corroded [19, 31, 32]. EIS response of 40Nd magnet plot (Figure 8) was similar

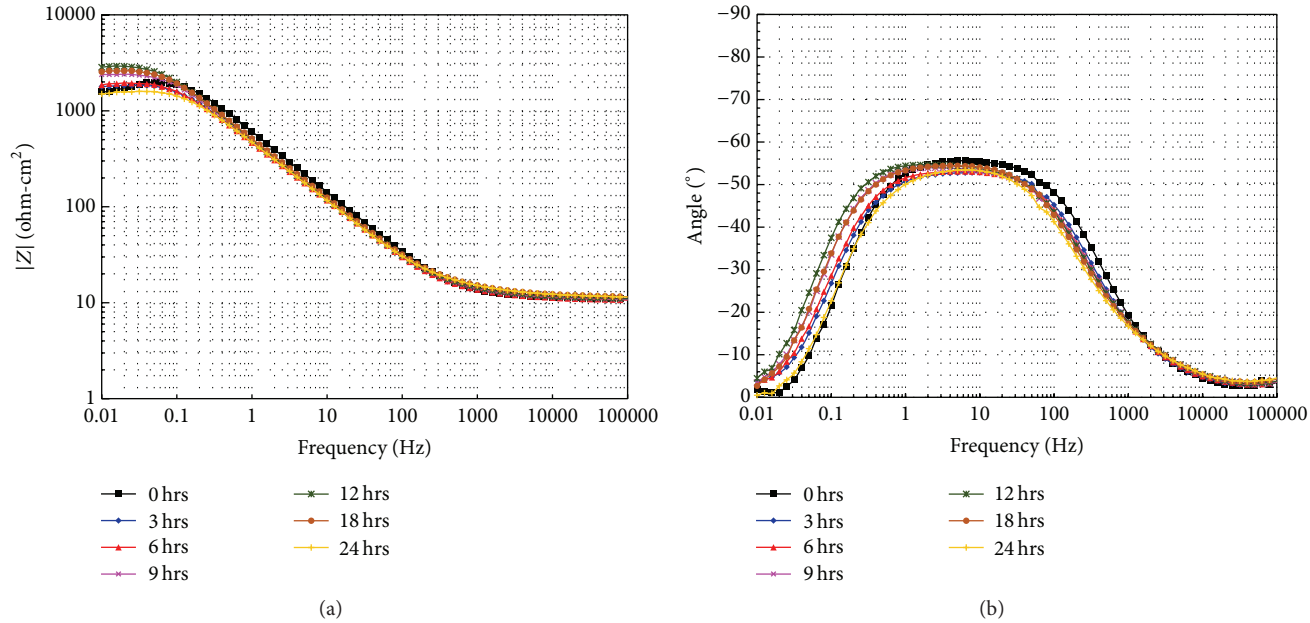

Figure 11: Bode plots for 30Nd8Pr magnet tested in 3.5% NaCl solution at 25°C for 24 hours.

to the 35Nd; however the main differences were as follows: the time constant observed in the intermediate frequency region (around 100 Hz) has a higher phase angle value and the second one observed in lower frequency has a more stable behavior; that is, only slight variations in the phase angle value and position were observed; however the phase angle value was minor (40–45°). The behavior observed in the low frequency region was similar; that is, impedance module decreases as time elapses. Again, this indicates the nonprotective nature of the protective layers formed onto magnet surface. This behavior is due to the higher content of Nd which increased the corrosion rate of the magnet through reactions (3) and (4). The amount of hydroxides formed onto surface was higher (time constant around 100 Hz) but was not able to form a stable passive film because chloride ions migrated to the interface and increased the dissolution of the magnet (low value of the second time constant and lower impedance modulus values). Co addition to the 40Nd magnet (Figure 9) showed a better performance. Apparently at time 0 hours only one time constant is observed around 20 Hz; however, as time passes, the shape of the phase angle spectrum is not according to a Gaussian distribution. The width of the spectrum is located from the high frequency region to the low frequency region. This suggests the presence of two time constants, where one of them (a slimy film) is in contact with the electrolyte and the other one (oxide film) is in contact with the magnet. Furthermore, phase angle values decrease from 68° to 56°, and this is associated with a decrease in the slope of the relationship $\log f - |Z|$. Notwithstanding this, the values are higher than those observed without the Co addition. This emphasizes the fact that the presence of cobalt improved the performance of the magnet favoring the formation of a more stable protective film which limited the diffusion of chloride ions into the interface.

Results in Bode format of EIS tests, for the NdPr magnets in 3.5% NaCl solution at 25°C for 24 h, are presented in Figures 10–12. The evolutions of the spectra are similar to those observed in the case of Nd magnets. In the case of 30Nd6Pr magnet (Figure 10), at the beginning of the corrosion process, the presence of a time constant between both high and intermediate frequency region is observed. But, as time elapses, the evolution of a second time constant is observed at frequencies below 1 Hz. This behavior may be because the presence of Pr increased the corrosion process and the rapid formation of a film of hydroxides on the surface of the magnet; however chloride ions were adsorbed and diminished the protective ability of the passive film, as can be seen from the evolution of the maximum phase angle value which tends to decrease as time passes [19, 31, 32]. It is observed that by increasing the Pr content (Figures 11 and 12) the maximum value of the phase angle shifts toward lower frequencies and its value slightly decreases as time passes. The shape of the phase angle spectrum is not according to a Gaussian distribution, and the width of the spectrum is located from the intermediate frequency region to the low frequency region. This suggests the presence of two time constants, as it has been explained above. The shift of the phase angle spectrum toward lower frequencies can be associated with a detachment, or thinning of the protective films [29, 30]. Hence, the protective layers formed onto magnet surface are nonprotective and favor the absorption of the chloride ions.

The superficial aspects of the Nd magnets tested in 3.5% NaCl solution at 25°C for 24 hours are shown in Figure 13. From the micrographs it can be seen that the surface attack was higher at increased Nd content (35 to 40Nd) since it is possible to observe the presence of areas with big pits. However, for the same Nd content but with the addition of

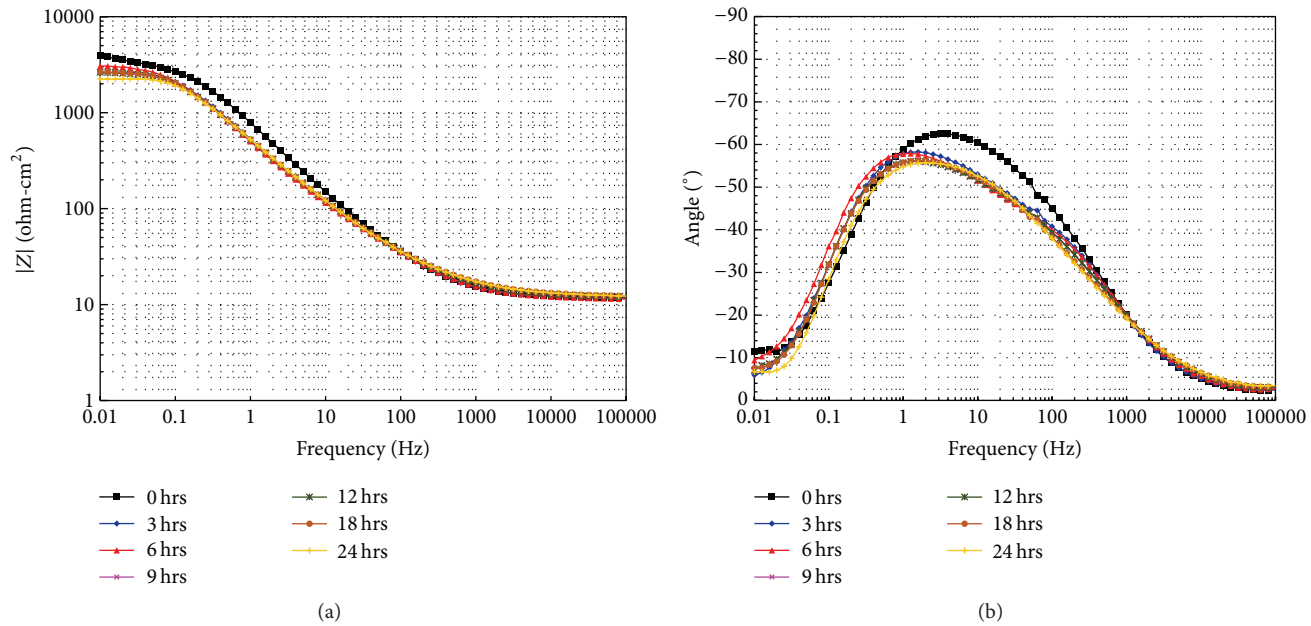

FIGURE 12: Bode plots for 30Nd10Pr magnet tested in 3.5% NaCl solution at 25°C for 24 hours.

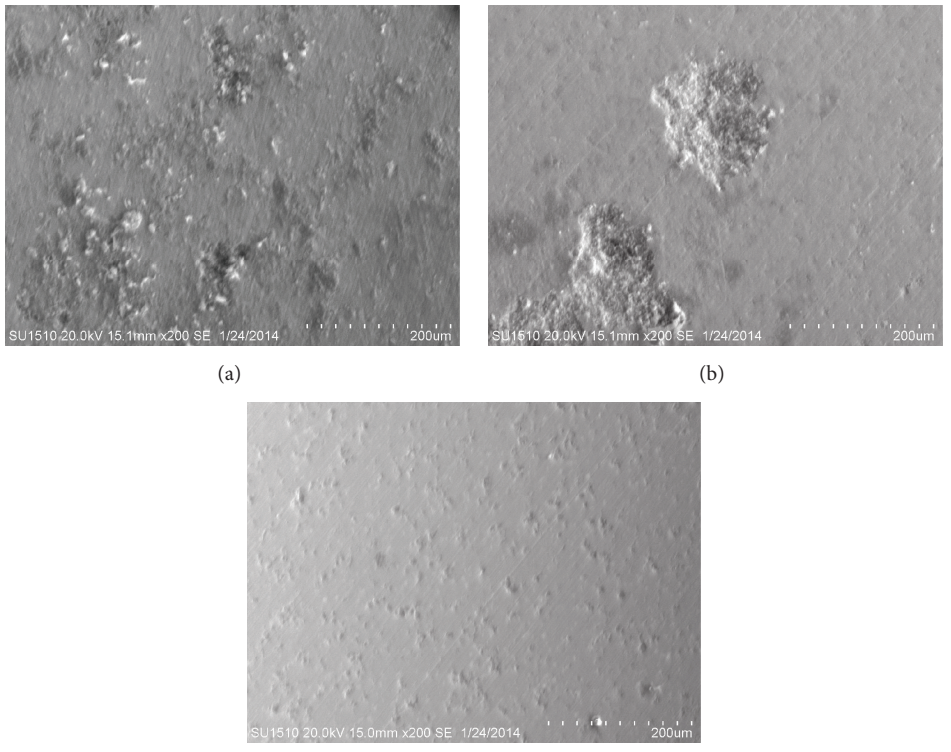

FIGURE 13: Superficial aspects of Nd magnets after corrosion tests for 24 hours in 3.5% NaCl solution at 25°C: (a) 35Nd, (b) 40Nd, and (c) 40Nd3Co.

Co, the surface appearance is completely different; in this case the presence of big pits was not observed, and instead the presence of small pits along what appears to be the grain boundaries was observed. Observations indicate that increasing the Nd content increases the corrosion rate and the adding of Co enhances the corrosion resistance. It is said that Co is added to replace iron and in order to increase the Curie temperature and the corrosion resistance of the magnets, and the corrosion resistance is due to the presence of the Nd_3Co phase which occurs at both grain boundaries

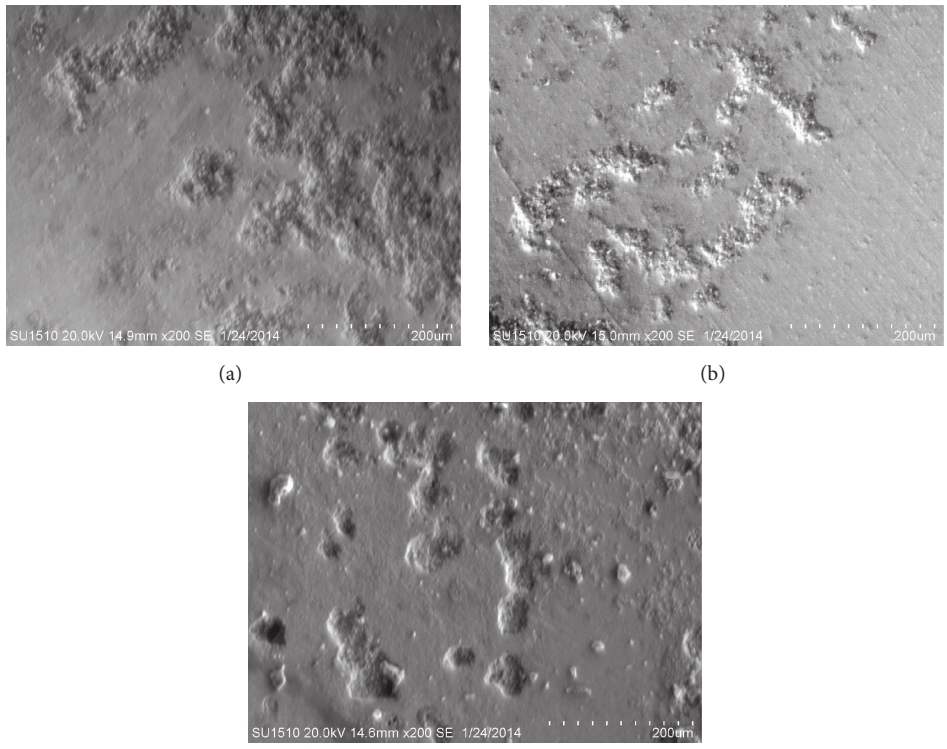

(a) (b)

(c)

Figure 14: Superficial aspects of NdPr magnets after corrosion tests for 24 hours in 3.5% NaCl solution at 25°C: (a) 30Nd6Pr, (b) 30Nd8Pr, and (c) 30Nd10Pr.

and triple junctions [33]. The superficial aspects of NdPr magnets tested in 3.5% NaCl solution at 25°C for 24 hours are shown in Figure 14. According to the micrographs, the magnets showed pitting attack and increasing the Pr content increased the pit depth, although the affected area was more localized. Again, these results indicate that the Pr addition increases the corrosion rate of Nd magnets and apparently enhances the pitting attack.

Figures 15 and 16 show the optical micrographs of the Nd magnets and NdPr magnets. The micrographs show the presence of the main phases, namely, $Nd_2Fe_{14}B$ main phase and Nd-rich grain boundary phase, as well as small amount of intergranular B-rich phase in all the samples, and almost all the grains are squares with facetted surfaces. From Figure 15, it is observed that an increase in the Nd concentration caused a decrease in grain size of the $Nd_2Fe_{14}B$ phase and consequently increased the grain boundaries and the grain junctions where the Nd-rich phase is located. It is known that the Nd-rich phase enhances densification during the sintering process and decreases the number of nucleation sites, but it is preferentially attacked [34, 35]. Moreover, with the Co addition, a grain coarsening effect of the $Nd_2Fe_{14}B$ phase is observed, which may contribute to increasing the corrosion resistance. Warren et al. found that the Co addition resulted in the formation of little or no Nd-rich phase, being replaced with Nd-Co precipitates [36].

On the other hand, from Figure 16 it can be observed that the Pr addition increased the grain boundaries (Nd-rich phase) and the amount of intergranular phases. Similar observations were obtained by Pandian et al., when they evaluated the effect of Nb addition on the microstructural features magnets [37]. Therefore, the corrosion resistance of the NdPr magnets decreased. This is consistent with studies about the effect of doping elements on the magnetic properties and microstructural features of magnets; it was found that the dopant element concentration is much higher in the Nd-rich phase. Moreover, the complexity of the intergranular region increases with additive elements, and at least one additional phase is clearly identified [37–39]. Therefore, in order to increase the corrosion resistance of the magnets, the Nd-rich phase should be as low as possible.

From the above results, it is possible to define the appropriate equivalent circuits (EC) in order to analyze the impedance spectra. The equivalent circuits, fitted to the impedance data, calculate the electrochemical parameters of interest, such as electrolyte resistance (R_s), charge transfer resistance (R_{ct}), and double layer capacitance (C_{dl}). From the spectra data, if a nonideal frequency response is clear, it is common to employ distributed circuit elements as the

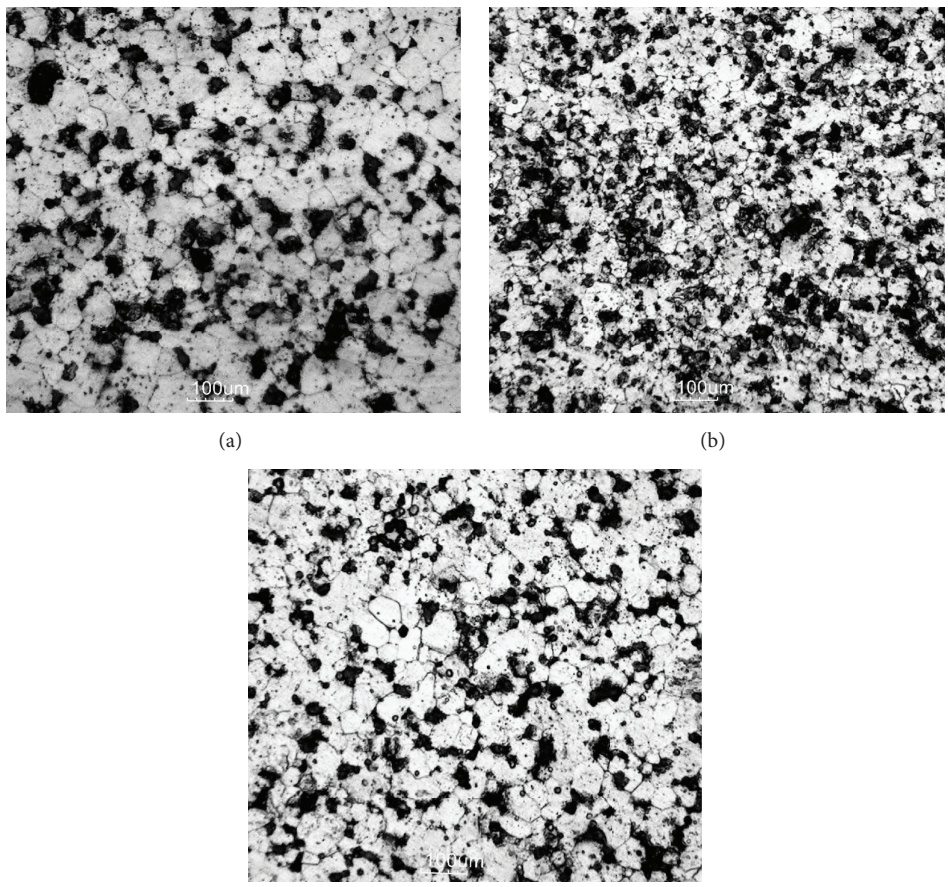

(a) (b) (c)

Figure 15: Optical micrographs of Nd magnets: (a) 35Nd, (b) 40Nd, and (c) 40Nd3Co.

constant phase element (CPE). CPE is used to compensate the inhomogeneity in the system, and it is an element whose impedance value is defined as

$$Z_{\mathrm{CPE}} = \frac{1}{Y_0}(i\omega)^{-n}. \tag{10}$$

Y_0 is a proportional factor; i is an imaginary number ($\sqrt{-1}$); ω is defined as the angular frequency ($\omega = 2\pi f$), f being the frequency; and n is related to the slope of the log $|Z|$ versus log f plots, and its value varies between 0.5 and 1. If $n = 1$, the CPE describes an ideal capacitor with Y_0 being equal to the capacitance (C); if $0.5 < n < 1$ describes a distribution of dielectric relaxation times in frequency space and if $n = 0.5$ the CPE represents a Warburg impedance with diffusional character.

As discussed previously, from 3 to 24 hours the impedance spectra indicate the presence of two time constants; therefore the impedance plots can be analyzed according to the CE shown in Figure 17. The first time constant represents a surface layer (reaction products which accumulate onto the surface of the magnets, according to reactions (3) and (4)), where R_f is the resistance of the film, and the second time constant represents the charge transfer process of the metal dissolution or the oxide dissolution, where R_{ct} describes the charge transfer resistance and $\mathrm{CPE}_{\mathrm{dl}}$ the constant phase element relating to the double layer capacitance. For the impedance spectra corresponding to 0 hours, the same model was used, but excluding the first time constant.

Figure 18 shows the variation of I_{corr} values versus time for the magnets evaluated. The calculation of I_{corr} was realized using Stern-Geary expression (see (2)), with R_{ct} values obtained modeling the impedance spectra and b_a and b_c values reported in Tables 1 and 2. Comparing Figure 18 with Figures 5 and 6, the similitude between I_{corr} values calculated from the EIS measurements and those calculated from LPR measurements is observed. This suggests that the equivalent circuits proposed are suitable to simulate the impedance spectra and are consistent with the effect of the chemical composition of the magnets, previously discussed.

Other parameters of interest determined from modeling of EC are shown in Figures 19–21. Figure 19 shows the variation of R_f for each simulated condition. R_f values represent the resistance of electrochemical species transporting to and from the magnet surface and electrolyte, and Rf values are proportional to the thickness of the path

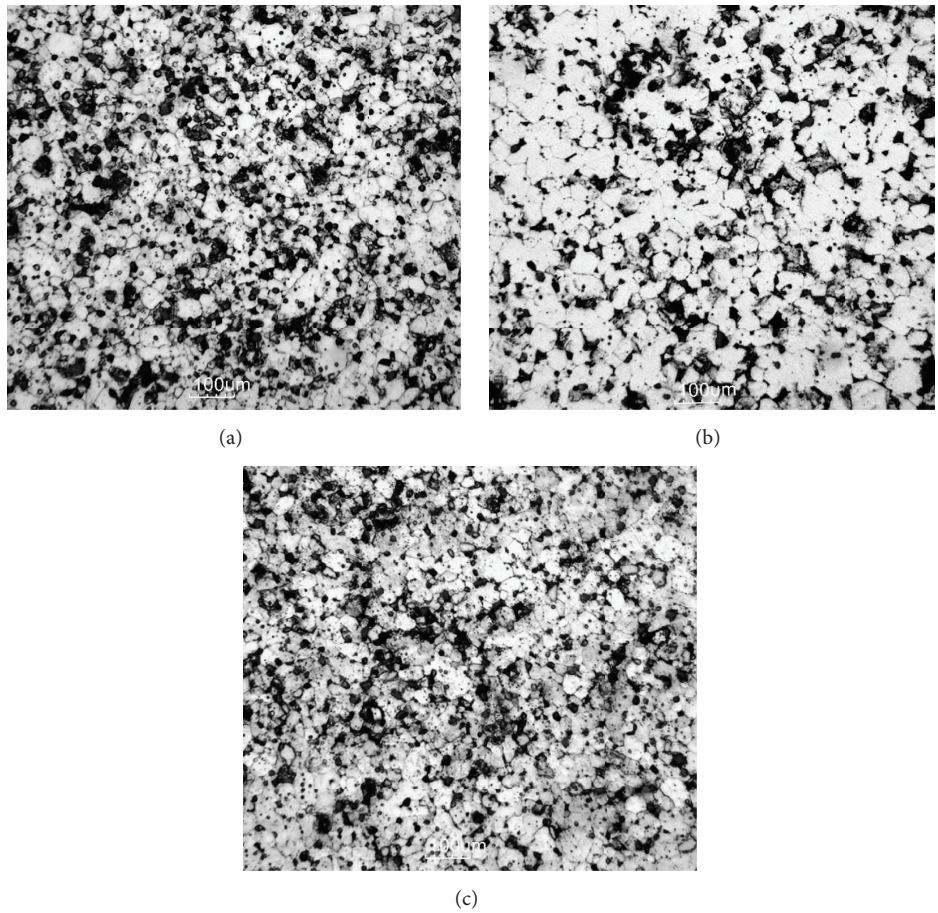

(a) (b) (c)

Figure 16: Optical micrographs of NdPr magnets: (a) 30Nd6Pr, (b) 30Nd8Pr, and (c) 30Nd10Pr.

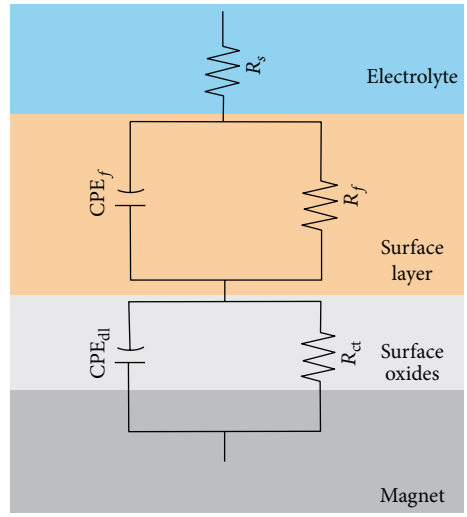

Figure 17: Equivalent circuit for permanent magnets corroded in 3.5% NaCl solution at 25°C from 3 to 24 hours.

in which electrochemical species diffuse. That is, the R_f values can be associated with the thickness of the layer of corrosion products formed. The trend of R_f values shows that increasing the concentration of Nd and Pr the slope of the curves increases, and therefore the amount of corrosion products formed. Moreover, the magnet with Co shows a stable trend which can indicate a lower corrosion rate. Figure 20 shows n_{ct} and n_f variation against time for each simulated condition. From n_{ct} values, it is observed that the corrosion process is controlled by charge transfer ($n_{ct} > 0.8$).

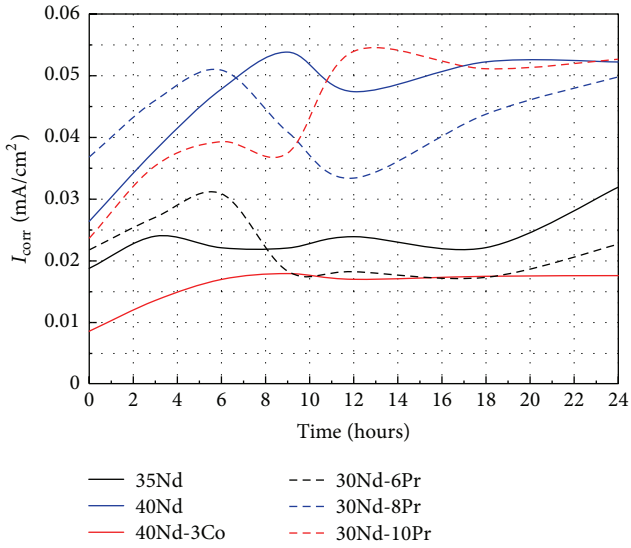

FIGURE 18: I_{corr} variation against time for the tested magnets. Determined from R_{ct} values of EIS measurements.

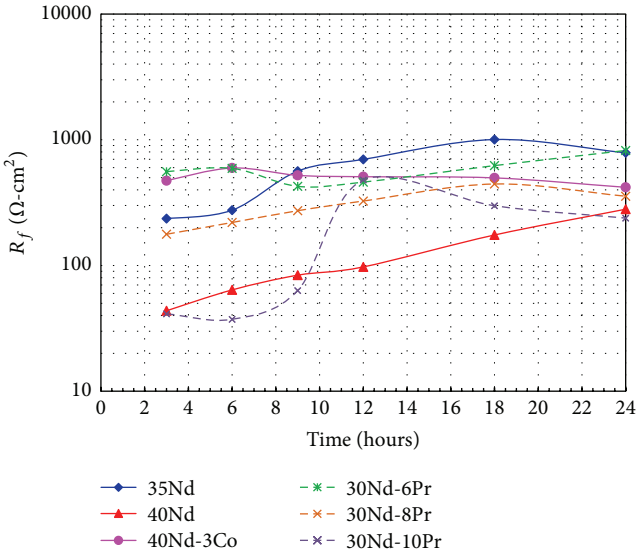

FIGURE 19: R_f variation against time for the tested magnets.

However, 35Nd, 40Nd, and 30Nd-10Pr magnets showed n_f values tending to 0.5 ($n_{ct} \rightarrow 0.5$); no diffusion processes were observed possibly because the corrosion products are easily dissolved into the bulk solution.

Figure 21 shows plots of the capacitance versus time for each simulated condition. Capacitance values were obtained from Y_0 values (see (10)) according to the following equation [40]:

$$C_i = \left(Y_{0i} R_i^{(1-n_i)}\right)^{1/n_i}. \quad (11)$$

From Figure 21 it is observed that the capacitance (C_{dl}) values are increasing with Nd and Pr content of the magnets; on the other hand, the capacitance (C_{dl}) values with low content of Nd and Co are lower. Same behavior is observed from the figure of capacitance film. However, C_f values are similar (same magnitude order) to those of C_{dl}. This indicates that the layer of corrosion products is not protective. It has been said that a decrease in the capacitance occurs if a surface layer (low dielectric constant) replaces the adsorbed water molecules (high dielectric constant) onto the metallic surface [41].

4. Conclusions

A study on the effect of the content of Nd, Pr, and Co in the corrosion behavior of permanent magnets in 3.5% NaCl solution has been carried out using electrochemical measurements. Results obtained from potentiodynamic polarization curves, open-circuit potential, linear polarization resistance, and electrochemical impedance spectroscopy measurements

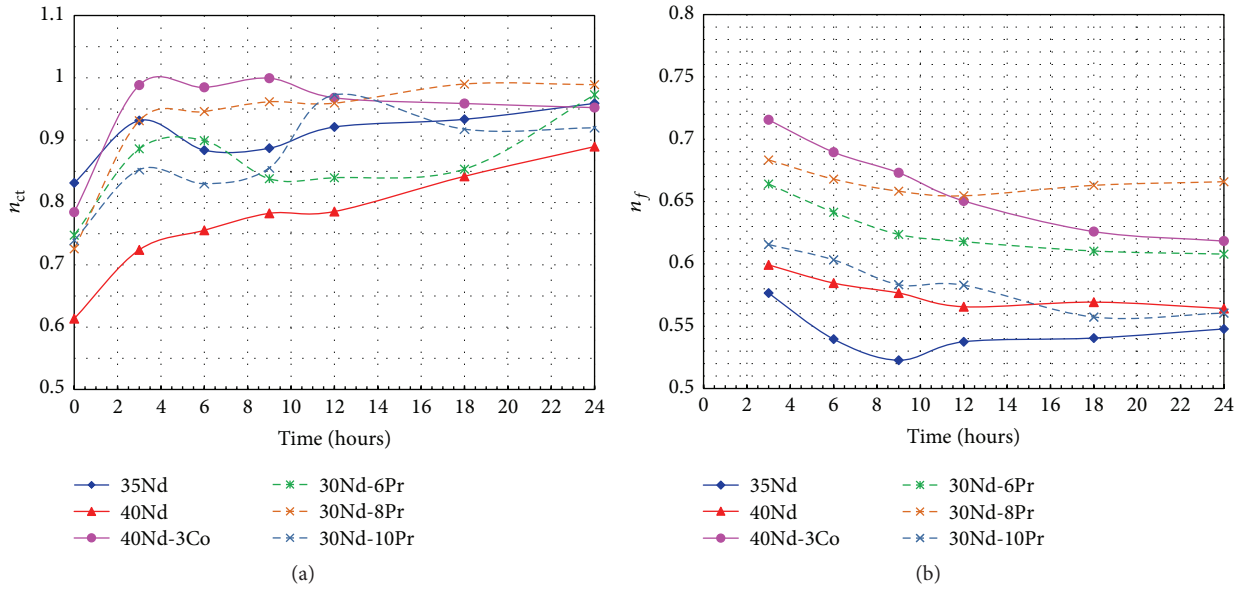

FIGURE 20: n_{ct} and n_f variation against time for the tested magnets.

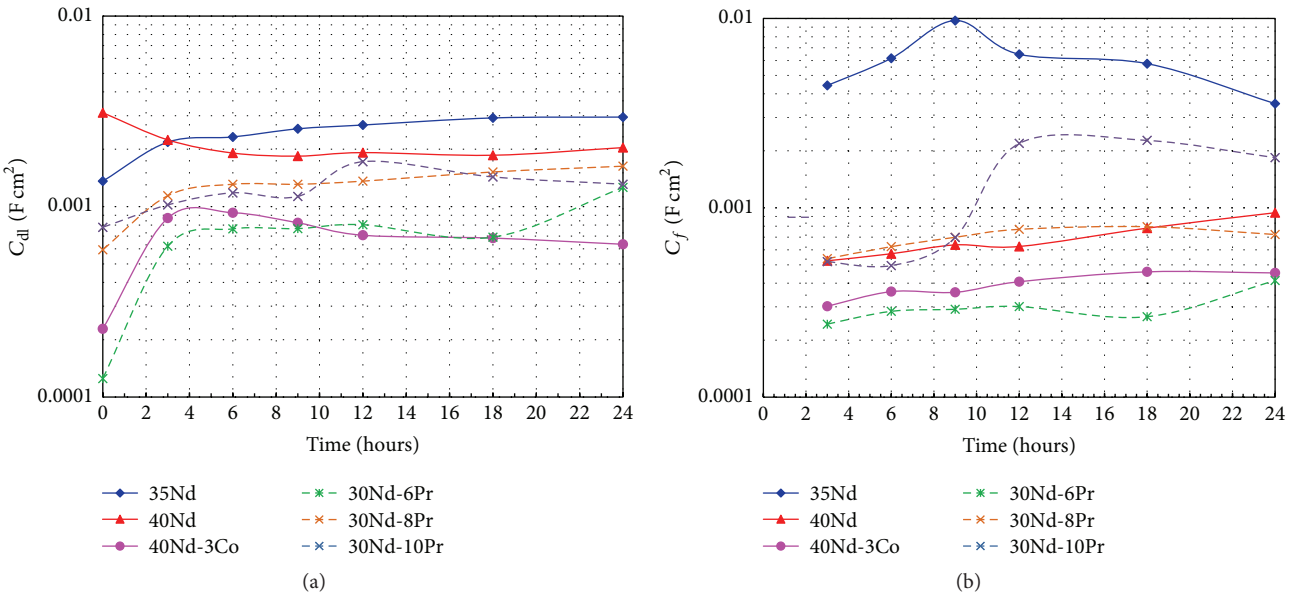

FIGURE 21: C_{dl} and C_f variation against time for the tested magnets.

were consistent. All the electrochemical corrosion indicated that the magnets showed an active corrosion process. Corrosion rate is increased by increasing the Nd content, but the Co addition enhances the corrosion resistance. For the same Nd content the Pr addition improves the corrosion resistance, but increasing the Pr content increases the corrosion rate. Results were consistent with the observations carried out by scanning electron microscopy, showing that the main mode of attack of the magnets is pitting, where the addition of Co reduces it, while the presence of Pr increases it.

Conflict of Interests

The authors declare that there is no conflict of interests regarding the publication of this paper.

Acknowledgments

Financial support from Consejo Nacional de Ciencia y Tecnología (CONACYT, Mexico) (Projects 196205, 159898, and 159913) is gratefully acknowledged. S. Godavarthi is thankful

to the postdoctoral scholarship from Dirección General de Asuntos del Personal Académico of the Universidad Nacional Autónoma de Mexico (DGAPA-UNAM).

References

[1] D. F. Cygan and M. J. McNallan, "Corrosion of NdFeB permanent magnets in humid environments at temperatures up to 150°C," *Journal of Magnetism and Magnetic Materials*, vol. 139, no. 1-2, pp. 131–138, 1995.

[2] M. Sagawa, S. Fujimura, N. Togawa, H. Yamamoto, and Y. Matsuura, "New material for permanent magnets on a base of Nd and Fe," *Journal of Applied Physics*, vol. 55, no. 6, pp. 2083–2087, 1983.

[3] I. Gurappa, "Corrosion characteristics of permanent magnets in acidic environments," *Journal of Alloys and Compounds*, vol. 360, no. 1-2, pp. 236–242, 2003.

[4] D. S. Edgley, J. M. Le Breton, S. Steyaert, F. M. Ahmed, I. R. Harris, and J. Teillet, "Characterisation of high temperature oxidation of Nd–Fe–B magnets," *Journal of Magnetism and Magnetic Materials*, vol. 173, no. 1-2, pp. 29–42, 1997.

[5] A. A. El-Moneim and A. Gebert, "Electrochemical characterization of galvanically coupled single phases and nanocrystalline NdFeB-based magnets in NaCl solutions," *Journal of Applied Electrochemistry*, vol. 33, no. 9, pp. 795–805, 2003.

[6] L. Schultz, A. M. El-Aziz, G. Barkleit, and K. Mummert, "Corrosion behaviour of Nd-Fe-B permanent magnetic alloys," *Materials Science and Engineering A*, vol. 267, no. 2, pp. 307–313, 1999.

[7] J. Fidler, "On the role of the ND-rich phases in sintered ND-FE-B magnets," *IEEE Transactions on Magnetics*, vol. 23, no. 5, pp. 2106–2108, 1987.

[8] S. A. Attanasio and R. M. Latanision, "Corrosion of rapidly solidified neodymium-iron-boron (Nd–Fe–B) permanent magnets and protection via sacrificial zinc coatings," *Materials Science and Engineering A*, vol. 198, no. 1-2, pp. 25–34, 1995.

[9] M. Rada, A. Gebert, I. Mazilu et al., "Corrosion studies on highly textured Nd-Fe-B sintered magnets," *Journal of Alloys and Compounds*, vol. 415, no. 1-2, pp. 111–120, 2006.

[10] S. Mao, H. Yang, Z. Song, J. Li, H. Ying, and K. Sun, "Corrosion behaviour of sintered NdFeB deposited with an aluminium coating," *Corrosion Science*, vol. 53, no. 5, pp. 1887–1894, 2011.

[11] J. L. Xu, Z. C. Zhong, Z. X. Huang, and J. M. Luo, "Corrosion resistance of the titania particles enhanced acrylic resin composite coatings on sintered NdFeB permanent magnets," *Journal of Alloys and Compounds*, vol. 570, pp. 28–33, 2013.

[12] V. A. Yartys, A. J. Williams, K. G. Knoch, P. J. McGuiness, and I. R. Harris, "Further studies of anisotropic hydrogen decrepitation in $Nd_{16}Fe_{76}B_8$ sintered magnets," *Journal of Alloys and Compounds*, vol. 239, no. 1, pp. 50–54, 1996.

[13] R. Sueptitz, M. Uhlemann, A. Gebert, and L. Schultz, "Corrosion, passivation and breakdown of passivity of neodymium," *Corrosion Science*, vol. 52, no. 3, pp. 886–891, 2010.

[14] H. H. Man, H. C. Man, and L. K. Leung, "Corrosion protection of NdFeB magnets by surface coatings—part 2: electrochemical behaviour in various solutions," *Journal of Magnetism and Magnetic Materials*, vol. 152, no. 1-2, pp. 47–53, 1996.

[15] B. Sprecher, Y. Xiao, A. Walton et al., "Life cycle inventory of the production of rare earths and the subsequent production of NdFeB rare earth permanent magnets," *Environmental Science and Technology*, vol. 48, no. 7, pp. 3951–3958, 2014.

[16] L. Cáceres, T. Vargas, and L. Herrera, "Influence of pitting and iron oxide formation during corrosion of carbon steel in unbuffered NaCl solutions," *Corrosion Science*, vol. 51, no. 5, pp. 971–978, 2009.

[17] G. Yan, A. J. Williams, J. P. G. Farr, and I. R. Harris, "The Effect of density on the corrosion of NdFeB magnets," *Journal of Alloys and Compounds*, vol. 292, no. 1-2, pp. 266–274, 1999.

[18] G. Yan, P. J. McGuiness, J. P. G. Farr, and I. R. Harris, "Environmental degradation of NdFeB magnets," *Journal of Alloys and Compounds*, vol. 478, no. 1-2, pp. 188–192, 2009.

[19] W. He, L. Zhu, H. Chen et al., "Electrophoretic deposition of graphene oxide as a corrosion inhibitor for sintered NdFeB," *Applied Surface Science*, vol. 279, pp. 416–423, 2013.

[20] X. Zhang, Y. Ma, B. Zhang et al., "Corrosion behavior of hot-pressed nanocrystalline NdFeB magnet in a simulated marine atmosphere," *Corrosion Science*, vol. 87, pp. 156–166, 2014.

[21] J. Porcayo-Calderon, O. Sotelo-Mazon, V. M. Salinas-Bravo, C. D. Arrieta-Gonzalez, J. J. Ramos-Hernandez, and C. Cuevas-Arteaga, "Electrochemical Performance of Ni20Cr coatings applied by combustion powder spray in $ZNCL_2$-KCL molten salts," *International Journal of Electrochemical Science*, vol. 7, no. 2, pp. 1134–1148, 2012.

[22] J. Porcayo-Calderon, C. D. Arrieta-Gonzalez, A. Luna-Ramirez et al., "Corrosion performance of Fe-Al intermetallic coatings in 1.0 M NaOH solution," *International Journal of Electrochemical Science*, vol. 8, no. 11, pp. 12205–12218, 2013.

[23] J. Porcayo-Calderon, L. M. Martínez de la Escalera, J. Canto, M. Casales-Diaz, and V. M. Salinas-Bravo, "Effect of the temperature on the CO_2-Corrosion of Ni_3Al," *International Journal of Electrochemical Science*, vol. 10, pp. 3136–3151, 2015.

[24] I. Gurappa, "Characterization of different materials for corrosion resistance under simulated body fluid conditions," *Materials Characterization*, vol. 49, no. 1, pp. 73–79, 2002.

[25] Y. Van Ingelgem, A. Hubin, and J. Vereecken, "Investigation of the first stages of the localized corrosion of pure copper combining EIS, FE-SEM and FE-AES," *Electrochimica Acta*, vol. 52, no. 27, pp. 7642–7650, 2007.

[26] M. F. López, A. Gutiérrez, and J. A. Jiménez, "In vitro corrosion behaviour of titanium alloys without vanadium," *Electrochimica Acta*, vol. 47, no. 9, pp. 1359–1364, 2002.

[27] Y. F. Zheng, B. L. Wang, J. G. Wang, C. Li, and L. C. Zhao, "Corrosion behaviour of Ti–Nb–Sn shape memory alloys in different simulated body solutions," *Materials Science and Engineering A*, vol. 438–440, pp. 891–895, 2006.

[28] J. E. G. González and J. C. Mirza-Rosca, "Study of the corrosion behavior of titanium and some of its alloys for biomedical and dental implant applications," *Journal of Electroanalytical Chemistry*, vol. 471, no. 2, pp. 109–115, 1999.

[29] L. M. Rivera-Grau, M. Casales, I. Regla et al., "Effect of organic corrosion inhibitors on the corrosion performance of 1018 carbon steel in 3% NaCl solution," *International Journal of Electrochemical Science*, vol. 8, no. 2, pp. 2491–2503, 2013.

[30] J. Porcayo-Calderon, M. Casales-Diaz, L. M. Rivera-Grau, D. M. Ortega-Toledo, J. A. Ascencio-Gutierrez, and L. Martinez-Gomez, "Effect of the diesel, inhibitor, and CO2additions on the corrosion performance of 1018 carbon steel in 3% NaCl solution," *Journal of Chemistry*, vol. 2014, Article ID 940579, 10 pages, 2014.

[31] X. Yang, Q. Li, S. Zhang, H. Gao, F. Luo, and Y. Dai, "Electrochemical corrosion behaviors and corrosion protection properties of Ni–Co alloy coating prepared on sintered NdFeB

permanent magnet," *Journal of Solid State Electrochemistry*, vol. 14, no. 9, pp. 1601–1608, 2010.

[32] J. B. Bessone, D. R. Salinas, C. E. Mayer, M. Ebert, and W. J. Lorenz, "An EIS study of aluminium barrier-type oxide films formed in different media," *Electrochimica Acta*, vol. 37, no. 12, pp. 2283–2290, 1992.

[33] F. E. Camp and A. S. Kim, "Effect of microstructure on the corrosion behavior of NdFeB and NdFeCoAlB magnets," *Journal of Applied Physics*, vol. 70, no. 10, pp. 6348–6350, 1991.

[34] S. Sugimoto, "Current status and recent topics of rare-earth permanent magnets," *Journal of Physics D: Applied Physics*, vol. 44, no. 6, Article ID 064001, 11 pages, 2011.

[35] W. Q. Liu, M. Yue, D. T. Zhang, J. X. Zhang, and X. B. Liu, "Electrochemical corrosion behavior of Nd–Fe–B permanent magnets with modified microstructure," *Journal of Applied Physics*, vol. 105, no. 7, Article ID 07A709, 2009.

[36] G. W. Warren, K.-E. Chang, B.-M. Ma, and C. O. Bounds, "Corrosion behavior of NdFeB with Co and V additions," *Journal of Applied Physics*, vol. 73, no. 10, pp. 6479–6481, 1993.

[37] S. Pandian, V. Chandrasekaran, G. Markandeyulu, K. J. L. Iyer, and K. V. S. Rama Rao, "Effect of Al, Cu, Ga, and Nb additions on the magnetic properties and microstructural features of sintered NdFeB," *Journal of Applied Physics*, vol. 92, no. 10, pp. 6082–6086, 2002.

[38] H. Wang, A. Li, Y. Guo, M. Zhu, and W. Li, "The effect of element doping and heat treatment on the impact resistance of Nd-Fe-B sintered magnets," *Journal of Applied Physics*, vol. 103, no. 7, Article ID 07E119, 2008.

[39] W. Liu, C. Sun, M. Yue et al., "Improvement of coercivity and corrosion resistance of Nd-Fe-B sintered magnets by doping aluminium nano-particles," *Journal of Rare Earths*, vol. 31, no. 1, pp. 65–68, 2013.

[40] H. Ma, X. Cheng, G. Li et al., "The influence of hydrogen sulfide on corrosion of iron under different conditions," *Corrosion Science*, vol. 42, no. 10, pp. 1669–1683, 2000.

[41] A. Y. Musa, R. T. T. Jalgham, and A. B. Mohamad, "Molecular dynamic and quantum chemical calculations for phthalazine derivatives as corrosion inhibitors of mild steel in 1 M HCl," *Corrosion Science*, vol. 56, pp. 176–183, 2012.